Critical Analysis of Threshold Stresses in the Creep Mechanisms of a Powder Metallurgy Magnesium Alloy AZ31

JORGE A. DEL VALLE and OSCAR A. RUANO

In this work, tensile tests were conducted on two powder metallurgy materials based on the AZ31 magnesium alloy. The first material, named AZ31-PM, was processed using atomized powder, followed by isostatic cold compaction at 340 MPa, plus hot extrusion at 350 °C. The second material, named AZ31-PMCM, used metal powder that was cryomilled in liquid nitrogen environment and processed as for the AZ31-PM material. Creep mechanisms were analyzed in the range 300 °C to 400 °C based on the creep laws determined previously for ingot metallurgy AZ31. Two threshold stresses, one for grain boundary sliding and the other for slip creep, both independent of temperature, were introduced, providing a consistent description of creep for the different AZ31-based materials. The variations observed in threshold stresses in the AZ31-PM material were attributed to an inhomogeneous distribution of dispersoids and satisfactorily explained by a composite type model. This method of analyzing the data is compared with the traditional one in the literature, demonstrating that the dependence of the threshold stresses with the temperature, reported in those articles, could actually be derived from the method used rather than from a real physical effect.

https://doi.org/10.1007/s11661-020-05658-8
© The Minerals, Metals & Materials Society and ASM International 2020

I. INTRODUCTION

MAGNESIUM alloys are the lightest structural metallic materials. Their good specific mechanical properties drive their use in the transportation industry with the aim of replacing heavier components.[1] However, they also have limitations regarding the elastic modulus, low temperature ductility, corrosion resistance and low creep resistance at high temperatures, limiting its use in structural applications at temperatures > 150 °C. Therefore, in the past 10 years a considerable effort has been devoted to developing new alloys with the aim of improving these properties. Primarily, these efforts have been concentrated on processing new magnesium alloys by rare earth addition. Currently, creep resistant magnesium alloys contain relatively high amounts of yttrium and/or rare earth elements[2–5] and transition elements.[6–10] Another way to increase the yield strength, is to strengthen the material by a dispersion of oxides/particles made by powder metallurgy or metal matrix composite techniques.[11–15] The improvement of creep properties against high temperature is usually attributed to the presence of finely dispersed precipitates/particles that prevent the movement of dislocations. Therefore, introducing a dispersion of fine particles is an appropriate way to improve the creep resistance of magnesium alloys.

However, the presence of second-phase particles often carries an associated grain refinement effect that can have an adverse effect on the creep resistance. As is well known, the grain refinement encourages a grain boundary sliding (GBS) deformation mechanism at increasing strain rates. For example, GBS controls plastic deformation at strain rates of 10^{-4} s^{-1} at high temperatures in cast or forged AZ31 magnesium alloy with grain sizes < 20 μm.[16] In this case, it is possible to sustain high tensile elongations because of the low stress exponent of the related power creep law, phenomena termed *superplasticity*. In PM alloys with a microstructure that combines a fine grain size and dispersion of second-phase particles or oxides, the experimental evidence shows,[11–15] on one hand, that the presence of particles helps maintain a fine grain size at high temperatures favoring superplastic creep with a stress exponent $n = 2$ at high strain rates and stresses. However, on the other hand, data also show a sharp drop in the strain rates for a narrow range of low stresses. That is, very high stress exponents and low ductility are obtained for low stresses. It is common in the literature to attribute the behavior of high stress exponents to the presence of a

JORGE A. DEL VALLE and OSCAR A. RUANO are with the Department of Physical Metallurgy, CENIM-CSIC, Av. Gregorio del Amo 8, 28040 Madrid, Spain. Contact e-mail: ruano@cenim.csic.es
Manuscript submitted September 19, 2019.
Article published online February 19, 2020

threshold stress, which in most cases is reported to be grain size and temperature dependent.[11,12,17]

From the technological point of view this phenomenon is very interesting, because for a certain range of high stresses the material allows superplastic forming while for low stresses the material is highly creep resistant. From the point of view of the study of the deformation micromechanisms, the presence of a threshold stress, related to GBS, also is of great interest since the cause is not well understood at the present. GBS is accommodated by glide dislocations but the controlling mechanism of the GBS rate is the climb of dislocations at the tip of pile-ups in grain boundaries.[18] Particles can affect the slip creep because dislocations can suffer an attractive detachment stress,[19,20] but it is not well understood how this interaction could affect the rate of climb at the tip of these pile-ups.

In this article the inclusion of threshold stresses in the creep equations will be analyzed to explain the experimental data obtained in two materials, one with a heterogeneous microstructure, processed by powder metallurgy, based on the alloy AZ31.

The AZ31 alloy has the advantage of having been exhaustively studied in the form of rolled sheets. Recently, a complete review of the creep mechanisms that act at different temperatures and the influence of grain size has been published.[21] It is our intention to use this set of creep laws as a basis to analyze the powder metallurgy of AZ31 by introducing only a single constant threshold stress as an additional parameter in each of the creep equations corresponding to the principal mechanisms controlling the deformation rate, GBS and slip creep. In the case of the material with a heterogeneous microstructure, with the additional modeling as a composite material, the experimental results could be also explained with the same set of creep equations used in the homogeneous material.

II. MATERIALS AND EXPERIMENTAL PROCEDURE

In this work, two materials, named AZ31-PM and AZ31-PMCM, based on the AZ31 magnesium alloy, were processed by powder metallurgy methods. First, the alloy powder was obtained from AZ31 cast bars using the electrode induction-melting gas atomization (EIGA) technique. The average powder size was < 100 μm. From the atomized powder, the AZ31-PM material was processed through a path consisting of an isostatic cold compaction at 340 MPa, plus a hot extrusion at 350 °C with an extrusion ratio and rate of 1:25 and 0.4 mm s^{-1}, respectively.

In the case of the AZ31-PMCM material, the metal powder was cryomilled in liquid nitrogen environment using a Union Process attritor ball mill model 01HD. The milling conditions were: 1:10 ratio powder/balls mass, ball size 3/16″, milling speed 1000 r.p.m. and 1 hour milling time. Finally, the powders were consolidated as for the AZ31-PM material.

In addition, the mechanical behavior of both powder metallurgy materials was analyzed based on the available data on the cast and rolled AZ31 alloy. The data were collected from the literature and from our own experimental data published in previous works.[16,21,22]

The microstructures of the powder metallurgy materials in the different stages of processing were examined by optical microscopy (OM). The sample preparation consisted of grinding on SiC paper, followed by mechanical polishing with 6 and 1 μm diamond paste and final polishing using colloidal silica. The grain structure was revealed by subsequent etching using a solution of ethanol (100 ml), picric acid (2 g), acetic acid (2 ml) and water (5 ml). The grain size was determined by the linear intercept method, measuring about 1000 grains. The mean (true) grain size, d, was calculated from the mean intercept length using a 1.74 factor. Thin samples for transmission electron microscopy (TEM) observations were prepared by electropolishing using a solution of 25 pct nitric acid in methanol, and final thinning by ion milling.

The mechanical behavior was studied using tensile tests performed at temperatures of 300 °C, 350 °C and 400 °C and strain rates in the range 5×10^{-6} to 10^{-1} s^{-1}. Cylindrical dog-bone tensile samples of 10 mm gage length and a radius of 3 mm were machined out of the extruded bars with the tensile axis parallel to the extrusion direction. Tensile tests were performed at these different temperatures in a screw-driven testing machine equipped with a parabolic furnace. The heating time for temperature stabilization of the sample and grips was 30 minutes.

Two types of tensile tests were performed. Continuous tests at constant strain rate, and strain rate change tests using a constant strain rate up to the peak stress and then conducting the successive jumps to the different examined strain rates were carried out to obtain the steady-state stresses with minor changes in the microstructure.[16,23]

For additional investigation of the grain size effect on mechanical properties, some tensile samples of the AZ31-PM material were annealed for 60 minutes in an electric furnace previously to the tensile test at 400 °C and 450 °C and those for the AZ31-PMCM material at 450 °C and 500 °C. These samples are termed PM + HT400, PM + HT450, PMCM + HT450 and PMCM + HT500, respectively. In this way, the grain coarsens statically up to larger values. The mean grain sizes were determined before and after tensile testing by the linear intercept method to evaluate the dynamic grain growth.

III. RESULTS

A. *Microstructure of the AZ31PM and PMCM Materials*

Figure 1 shows optical micrographs, OMs, of the various materials and heat treatment conditions. Figures 1(a) and (b) shows the microstructure of the extruded PM and PMCM materials, respectively. Figures 1(c) and (d) shows the microstructure of the

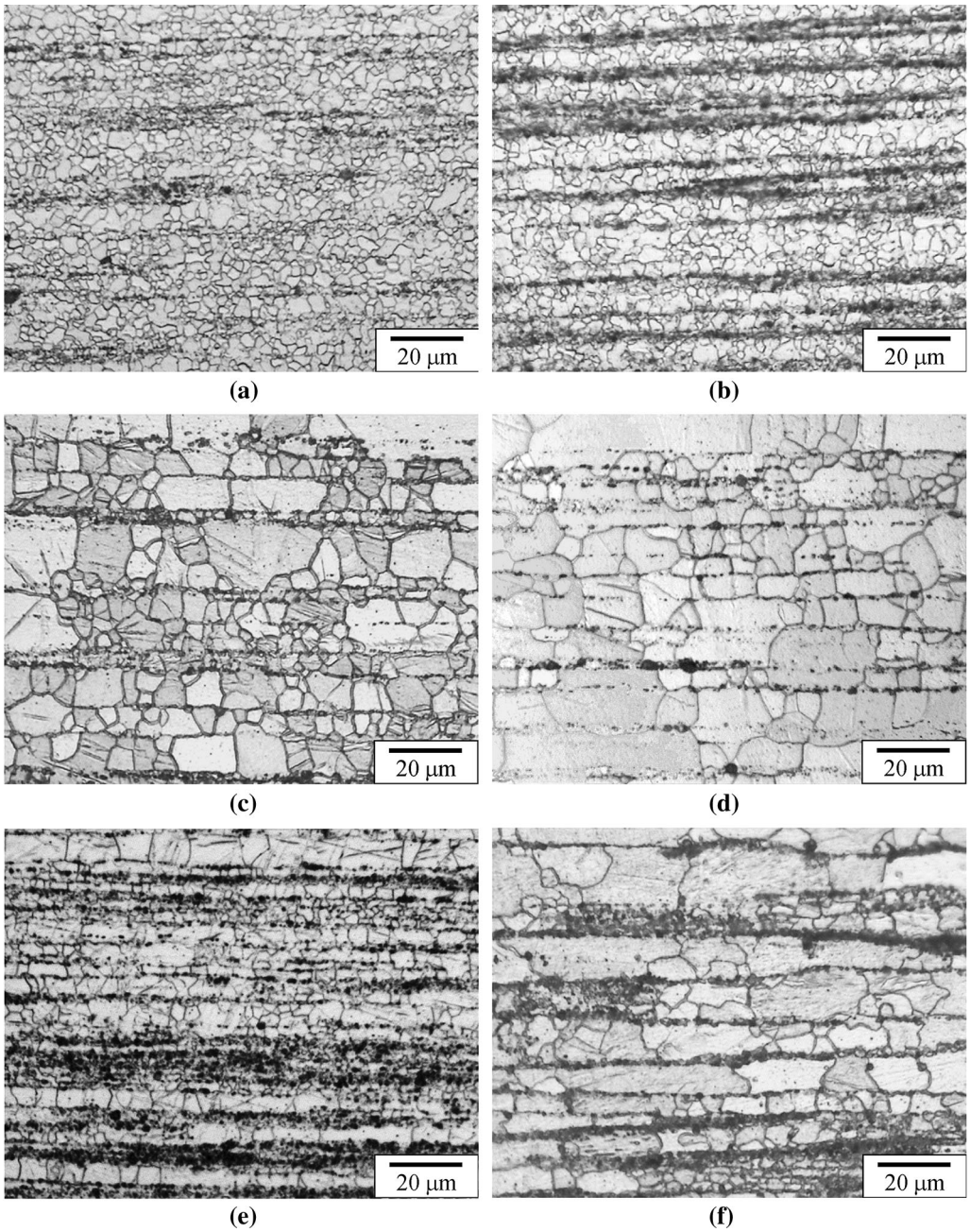

Fig. 1—Optical micrographs of the studied materials based on the AZ31 alloy: (*a*) PM, (*b*) PMCM, (*c*) PM + HT400, (*d*) PM + HT450, (*e*) PMCM + HT450 and (*f*) PMCM + HT500.

PM samples after 1 hour heat treatment consisting of a static annealing at 400 °C and 450 °C, respectively. Figures 1(e) and (f) shows OM of the PMCM samples after 1 hour heat treatment of a static annealing at 450 °C and 500 °C, respectively. The microstructure of the IM-AZ31 rolled and fully recrystallized material can be seen in previous works.[16,22]

Table I shows an overall coverage of the microstructural data. Values for the mean grain size of the materials are obtained after extrusion (as-extruded), after heat treatments, and measured at the gauge length of tensile samples after being tested in the mode strain rate change tests. Typically, these tests reach a low total strain of about 0.1 to 0.15. Once the stress corresponding to the highest test speed has been reached, completing the strain rate changes, the test is stopped without waiting for fracture. Most of the time spent in the test corresponds to the low strain rate of 2×10^{-5} s^{-1} (stage that lasts about 5 minutes).

As shown in Table I, the grain size of the annealed samples is quite stable during subsequent tensile tests.

The static annealing in the PMCM + HT450 samples did not produce significant changes in the microstructure with respect to the PMCM samples (Figures 1(b) and (e)). Therefore, tensile tests were not conducted after this treatment.

Table I. Microstructural Parameters of PM and PMCM Materials

AZ31—PM Samples	d (μm)	T (°C)	d (*) (μm)	d_f (μm)	d_{ox} (μm)	f_{ox}
PM	3	300	3	3	2.5	0.2
Fig. 1(a)		350	4	4	2.5	
		400	11.4	12	4	
PM + HT400	8.8	300	9.5	17	4	0.2
Fig. 1(c)		350	10.9	17	4	
		400	11.5	17	4	
PM + HT450	12.5	300	13.9	25	7	0.2
Fig. 1(d)		350	14.7	25	7	
		400	16.6	25	7	
PMCM	3	300	3		3	> 0.95
Fig. 1(b)		350	4.2		4.2	
		400	7.1		7.1	
PMCM + HT500	8.3	300	9.6		9.6	> 0.95
Fig. 1(f)		350	9.5		9.5	
		400	10		10	

Mean grain size of the as-processed materials, d. Mean grain size in the deformed zone after tensile tests performed at 300, 350 and 400 ºC, d(*). Grain size determined in zones free of oxide particles, d_f, and zones with oxide particles, d_{ox}. Volume fraction of zones with oxide particles f_{ox}.

As can be seen, the powder metallurgy cryomilled materials, AZ31-PM and PMCM, have a very similar grain size, close to 3 μm, as a result of the extrusion process at 350 °C. The grain size is stable during testing at 300 °C and 350 °C, while the grain grows during tests at 400 °C.

All powder metallurgy materials contained scattered particles of magnesium oxide, MgO. However, there are important differences in the distribution of MgO particles when PM and PMCM materials are compared. Figures 1(a) and (b) shows dark traces orientated in the extrusion direction in both PM and PMCM materials. These traces, with a high density of oxide particles, correspond to the oxide shell of the powder particles which become cracked when particles elongate during extrusion. In zones between these traces, the micrographs obtained by TEM show a greater presence of fine particles of magnesium oxide in the samples prepared from milled powder (Figure 2(b)) than in samples obtained from non-milled powders (Figure 2(a)).

From the observation of the microstructure by OM and TEM, a schematic description of the microstructure development and the distribution of oxide particles can be made as shown in Figure 3. During milling, oxide particles are forced into the material powders and then subsequent extrusion results in a PMCM material with a large amount of oxide particles and with a much higher homogeneous distribution than the PM material. On the other hand, AZ31-PM extruded bars made with as-received powders have fewer oxide particles arising from the oxide shells of powders, leading to an inhomogeneous distribution of the dispersoids. Grains that recrystallize close to or inside the traces, coincident with the surface of old powder particles, have oxide dispersoids inside the material, while grains recrystallized in zones between the traces should be free of oxide particles.

It should be noted that the microstructure difference, which gives the PM samples a duplex microstructure, but not the PMCM samples, is given by the distribution of fine oxide particles that cannot be seen by optical microscopy. As shown below, through optical microscopy an indirect inference of its presence due to the stability of the grain size during thermal annealing treatments can be made

B. *Microstructure Changes During Static Annealing Treatments*

Static annealing treatments were performed to produce grain coarsening. The evolution of grains depends on the distribution of oxide particles. In PMCM samples, due to the presence of oxide particles in all grains, grain coarsening was lower than in PM samples. For example, comparing PMCM and PM samples both treated at 450 °C (Figures 1(d) and (e)), these microstructures, which were initially very similar under the optical microscope, evolve very differently with the heat treatment. In PM samples, grain growth occurs rapidly in areas between oxide traces where the grains are free of oxide particles, thus revealing the heterogeneous distribution of these particles.

Thus, with the help of the mentioned static annealing treatment, it is possible to roughly determine the volume fraction of the areas containing oxide particles. In addition, two grain sizes, corresponding to zones with and without oxide particles, were determined by the linear intercept method, termed d_{ox} and d_f, respectively. The volume fraction of zones with dispersoids f_{ox} has been estimated from the areal fraction of the zones with fine grains over several dozens of optical micrographs of PM + HT400 samples. An estimation of about 0.2 is derived as given in Table I. It is assumed that all PM samples, independently of the heat treatment, have the same volume fraction.

In the case of PMCM samples, heat treatments at 400 and at 450 °C (Figure 1(e)) do not result in noticeable grain growth, except for minor zones. The fraction of these zones is < 5 pct of the total area indicating that the oxide particles are present in almost all the material.

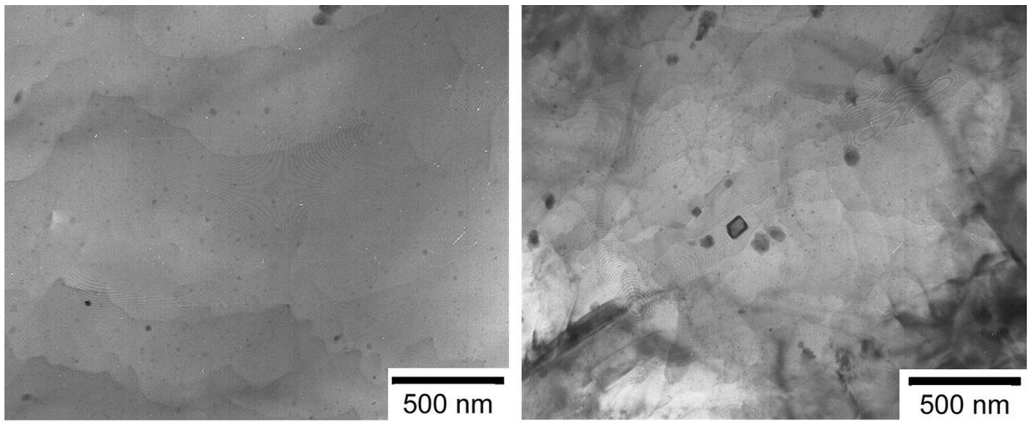

(a) (b)

Fig. 2—TEM micrographs of (*a*) PM and (*b*) PMCM samples, respectively.

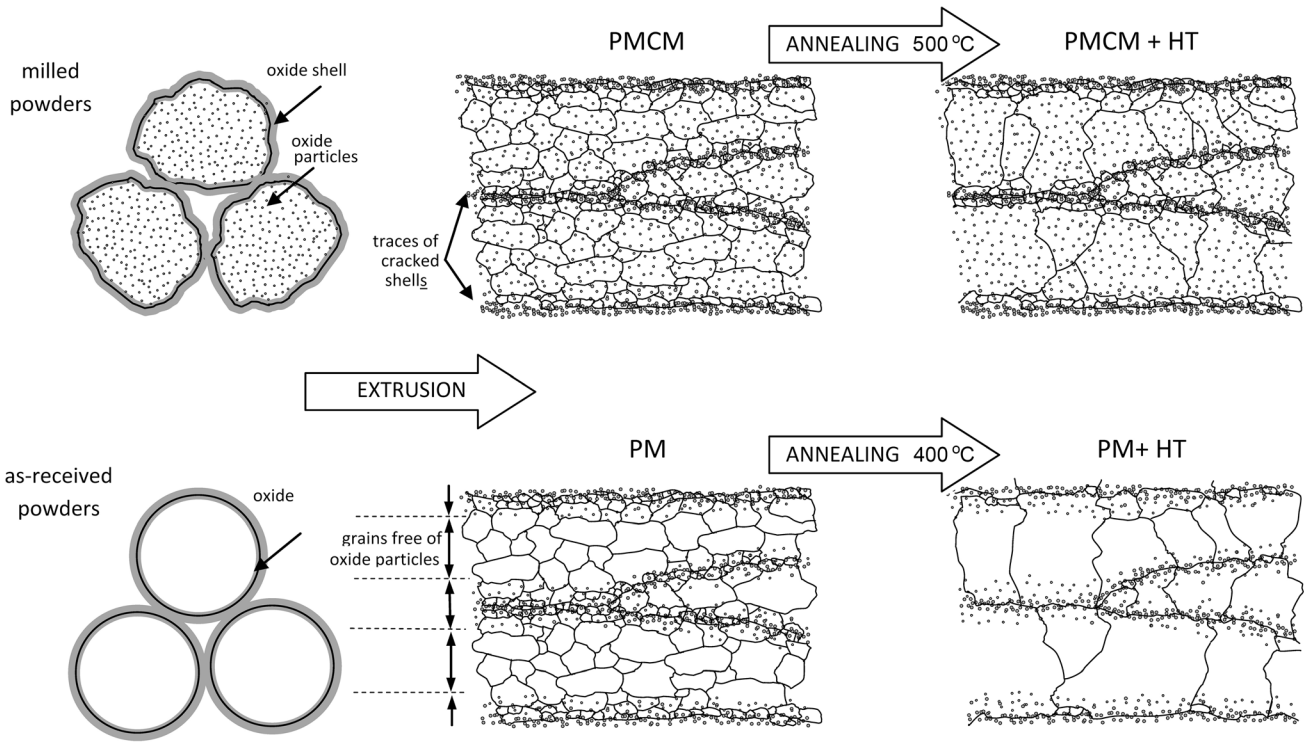

Fig. 3—Scheme of the microstructures and their evolution under annealing treatments for the PMCM and PM materials.

Therefore, it is not justified to treat the material as if it had a duplex microstructure. In the case of the heavy heat treatment at 500 °C (Figure 1(f)) the grains have grown up to the traces of the powder particles as described in Figure 3. This does not imply that the large grains in Figure 1(f) do not have oxide particles inside.

During coarsening, the grains develop a brick structure with squared-shaped grains (Figures 1(c) through (f) and schematically in Figure 3). In both PMCM and PM samples, traces of a dense amount of oxide particles form a barrier preventing the movement of the grain boundaries, even at the 500 °C. Grain boundaries tend to align parallel to these traces coincident with the extrusion direction. In the areas between the traces, the grain boundaries tend to align perpendicular to the extrusion direction (Figures 1(c) through (f) and Figure 3).

C. *Monotonic Tensile Tests and Strain Rate Change Tensile Tests*

Figures 4(a) and (b) shows tensile curves for tests performed at 300 °C, 350 °C and 400 °C at a strain rate of 10^{-3} and 5×10^{-5} s^{-1}, respectively, for the PM and PMCM materials. Unlike rolled samples,[16,22,24] powder metallurgy materials show little change in flow stress

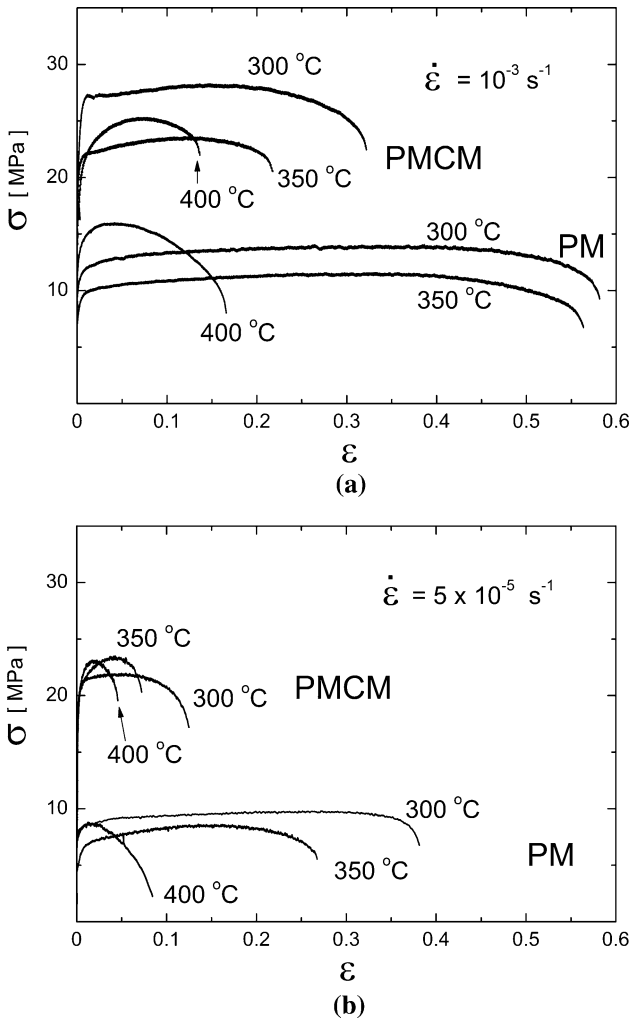

Fig. 4—Tensile curves of PM and PMCM materials at 300 °C, 350 °C and 400 °C for the strain rates (*a*) 10^{-3} s^{-1} and (*b*) 5×10^{-5} s^{-1}.

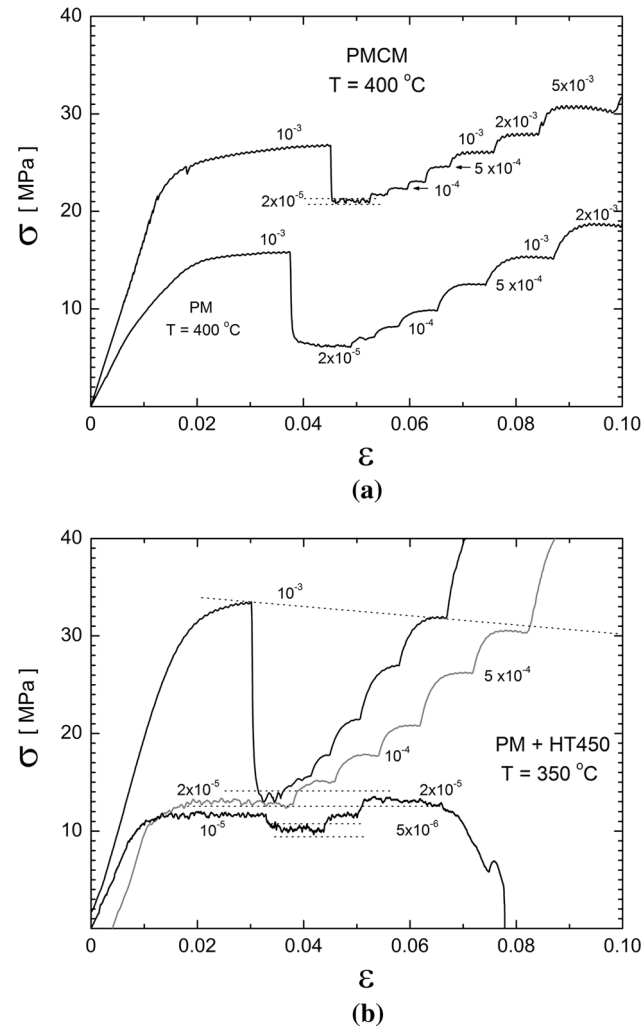

Fig. 5—Strain rate change tests. (*a*) Performed at 400 °C on samples of the PM and PMCM materials. (*b*) Performed at 350 °C on samples of the PM + HT450 material at different initial strain rates.

with temperature. The milling processing leads to a significant reduction in ductility and an increase of the flow stress for PMCM samples. During continuous tensile tests, Figure 4, curves at 400 °C show higher peak stress than curves at 350 °C. This effect is more important in PM samples that have fewer oxide dispersoids. As mentioned in Section III–A, the grain size is stable for the mechanical tests carried out at 300 °C and 350 °C, while the grain grows to values of about 7 to 12 μm when testing at 400 °C, Table I. Additionally, when GBS creep operates, an increase in flow stress is expected because of dynamic grain growth. Therefore, the higher peak stress of 400 °C testing temperature is evidence of the operation of creep by GBS.

In Figure 5(a), two examples of strain rate change tests at 400 °C, performed on samples of the PM and PMCM materials, are shown. Tests start in Figure 5 at 10^{-3} s^{-1} like those in Figure 4(a), and the changes in strain rate take place once the stress has reached the peak. Then, the strain rate is first decreased to 2×10^{-5} s^{-1}, and once the stress reaches a stationary value, the strain rate is increased in sudden steps, and values of the steady state stresses are obtained as a function of the strain rates with minor changes in the microstructure.

During the jumps, the rate of 10^{-3} s^{-1} is again passed, obtaining values close to the initial stresses, which is an indication of the thermal stability of the microstructure after reaching the peak stress and during the changes in strain rate. Therefore the grain growth detected in Figure 4(a) for tests at 400 °C must have occurred in the heating stage of the tensile test and in the first part of deformation, before reaching the peak stress.

Figure 5(b) shows several curves, corresponding to strain rate change tests performed on samples of the PM + HT450 material. Performing tests at 10^{-3} s^{-1} and then down to 2×10^{-5} s^{-1} or, alternatively, at 2×10^{-5} s^{-1} from the beginning and then increasing the strain rate, yields values close to the stress levels because of the strong microstructural stability of the annealed samples. In case of deformation at 2×10^{-5} s^{-1} or below, serrated flow stress is evident. In these cases, a range of flow stress was measured instead of a single value.

In Figure 6(a) the strain rate is represented as a function of stress for the PM and PMCM materials. The

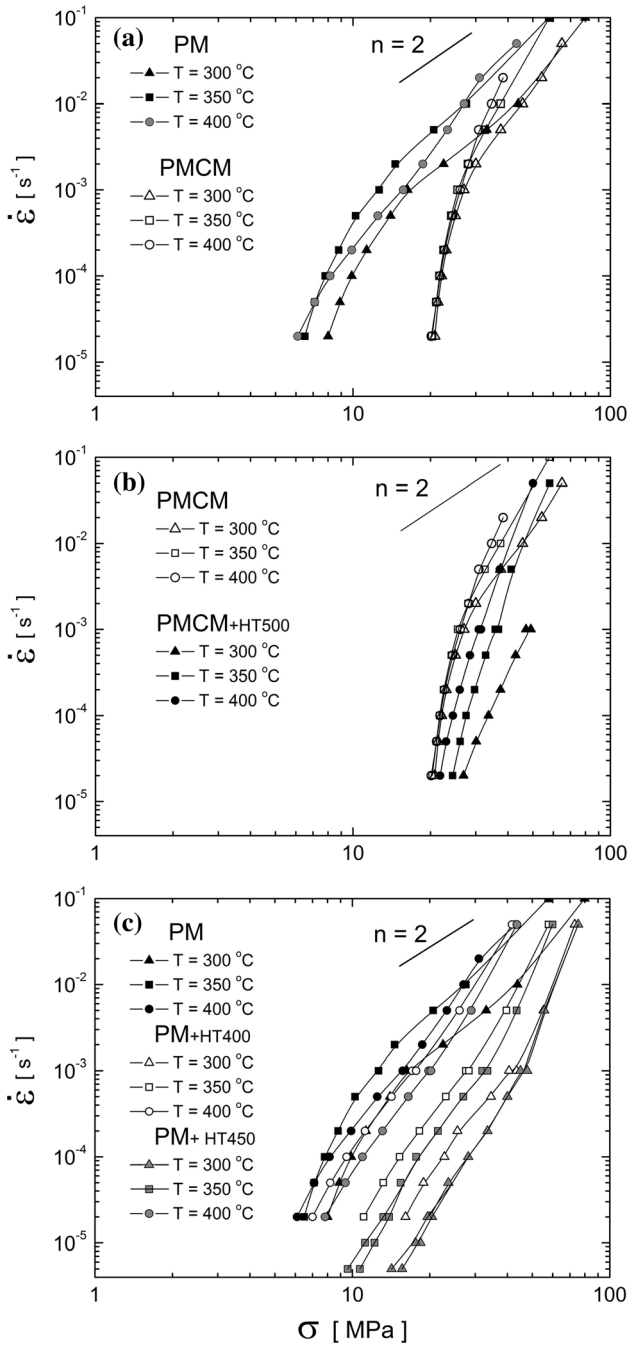

Fig. 6—Strain rate *vs* flow stress data. (*a*) Comparison of PM and PMCM materials tested in the same conditions. (*b*) Comparison of PMCM materials to show the effect of annealing at 500 °C. (*c*) Comparison of PM materials to show the effect of annealing at 400 °C and 450 °C.

effect of the annealing treatments is shown in Figures 6(b) and (c). The aforementioned serrated flow is depicted in Figure 6(c) by drawing two points for a given strain rate corresponding to the minimum and maximum stresses of the range. A power creep law type $\dot{\varepsilon} = k\sigma^n$ gives a linear behavior in a double log graph with a slope $n = 2$, related to the GBS mechanism, which is drawn as a visual guide in Figure 6.

IV. DISCUSSION

The present discussion will be carried out progressively, beginning in Section IV–A with a qualitative evaluation of the results shown in Figure 6. In Section IV–B the creep mechanisms for rolled AZ31 are reviewed. In Section IV–C the quantitative analysis of the data is started with the method usually applied in the literature, linear regressions in representations $\dot{\varepsilon}^{1/2}$ *vs* σ, which are insufficient to rationalize the data. In Section IV–D the case of PMCM mechanical behavior is analyzed on a phenomenological basis, introducing two threshold stresses for GBS and slip creep, as fitting parameters. In Section IV–E the case of the AZ31-PM material is analyzed considering the heterogeneity of this microstructure using a model for a composite-like material. Finally, Section IV–F shows that our analysis explains why the determinations performed by the method of linear regressions in Section IV–C lead to an apparent dependence on the temperature and grain size of the threshold stress.

A. *Qualitative Evaluation of the Data for AZ31-PM and AZ31-PMCM Materials*

Figure 6(a) highlights the importance of processing using mechanical cryomilling. Grinding made the PMCM material much more resistant at low strain rates than the PM material. Both materials show a region of drastic decrease in strain rate with a small decrease in stress. This decrease occurs for all temperatures, with the stresses tending to values of about 7 and 20 MPa for the PM and the PMCM materials, respectively.

In contrast, the flow stress of the two materials in the region of strain rates between 3×10^{-3} and 10^{-1} s^{-1} is similar. The stress exponent, n, has low values in this range, about two to three. Both powder metallurgy materials show their maximum ductility at high stresses in the strain rate range in which they have the lower stress exponent.

Creep is usually described by a diffusion-controlled dislocation creep equation, although other mechanisms may be important, for example, grain boundary sliding (GBS), which may in fact dominate deformation especially in fine grained materials. Each of these mechanisms is considered to operate independently of the others and has a particular dependence of the creep rate on the steady-state stress, temperature and the microstructural parameters expressed by a constitutive equation. The data presented in Figure 6 allow investigating the effect of the main microstructural features, grain size and oxide dispersion on the creep behavior of powder metallurgy materials:

1. The extruded PM and PMCM materials have the same grain size. Comparison of the two materials (Figure 6(a)) gives a clue about the role of oxide dispersoids.
2. The PMCM material has a more homogeneous distribution of oxide dispersoids. During annealing treatments, grain growth occurs, but it is assumed

that any contribution of oxide particles inside the grains and in their grain boundaries remains almost unaltered during annealing. Therefore, changes in mechanical behavior shown in Figure 6(b) for the PMCM + HT500 material should be attributed to a true grain size effect.

3. Figures 6(b) and (c) shows that the effect of the annealing treatment is stronger in the PM material compared with the PMCM material. At first glance, one might conclude that there is a greater effect of grain size on the PM material. However, this would be an incorrect conclusion because the importance of the heterogeneous microstructure of the PM material would be overlooked. This material consists of layers of grains with oxide particles and layers of grains free of dispersoids, as shown in Figure 3. Those grains can experience GBS like the grains in the AZ31 alloy prepared by conventional ingot metallurgy. Later, these results will be explained based on a composite model.

The third microstructural factor of interest in magnesium alloys is the texture.[23] In our case both, the powder metallurgy and the rolled IM-AZ31 materials have a basal fiber with basal planes parallel to the tensile direction. Therefore, the texture is not expected to introduce variations to be taken into account in the comparative analysis of the different materials presented here.

As is well known, GBS is a creep mechanism that depends on the grain size. This is the mechanism related to the stress exponent n = 2, which operates in the ingot metal (IM) and rolled AZ31 material for fine grain sizes, previously investigated in Reference 21. To perform a quantitative study of all data of the PM and PMCM materials, it is proposed in this work to rationalize the creep behavior of the powder metal samples using as a basis the creep equations describing the IM-AZ31 behavior with the addition of a minimum of new parameters, as will be shown in the following.

B. *The Creep Behavior of Rolled AZ31 Alloy as the Basis for the Rationalization of the Creep Behavior of PM AZ31*

A previous study,[21] after performing an exhaustive compilation of literature data for conventional IM-rolled AZ31 alloy, showed that the creep behavior can be described accurately by a set of equations, each responding to a particular mechanism dominant in certain ranges of stresses and temperatures. The GBS-controlled deformation mechanism is described by Eq. [1] in Table II. At high stresses, climb-controlled dislocation creep, described by Eq. [2], governs deformation. This last model was extended to larger stresses, including the power law breakdown (PLB) region, based on the Garofalo relationship (Eq. [3]). Table II gives the lattice (D_L) and grain boundary (D_{gb}) diffusivities, respective activation energies, Burgers vector and the Young modulus for magnesium. In Figures 7(a) and (b), a collection of literature data[12,22,25–38] is given for 300 and 400 °C for a broad range of grain sizes. It should be noted that the small grain size effect on the dislocation creep of AZ31 comes from the analysis of Spigarelli *et al.*[21] considering the creep data of > 30 papers. It is a matter of adjustments to have a good fit in the curves and not a basic assumption.

Although each one is dominant in a range of stresses, climb-controlled dislocation creep and GBS creep are independent deformation mechanisms that act in parallel. Therefore, the total strain rate is the sum of the two contributions:

$$\dot{\varepsilon}=k_4\left(D_{gb}/d^2\right)(\sigma/E)^2+k_8\{\sinh[\alpha(\sigma/E)]\}^5\left(D_L/b^2\right)(b/d)^p \quad [4]$$

The lines shown in Figures 7(a) and (b) correspond to Eq. [4] using the parameters given in Table II. The agreement is good for grain sizes < 50 μm. For the purpose of comparison, Figure 7 also presents data for coarse grain sizes ($d > 100$ μm) where n is > 2, and close to $n = 3$. As it was shown[21] data for the coarse grain size can be interpreted in terms of the solute-drag creep mechanism. However, at the fine grain sizes of the powder metallurgical samples, GBS is dominant over solute drag, and there is no need to consider the contribution of solute drag in our model of Eq. [4]. Finally, the most likely reason for the data scatter observed in Figures 7(a) and (b) for coarse materials is that microstructural changes, such as grain growth or recrystallization, are occurring during creep. To accurately adjust the elevated temperature flow data to a constitutive equation, the actual grain size at the strain used should be taken into account. However, the grain size is not a controlled parameter in most creep tests,

Table II. Constitutive Equations for Creep in AZ31 Tested in Ref. [21]

Creep Process	Equations [1], [2], and [3]	AZ31 Parameters Ref. [21]
Grain Boundary Sliding	$\dot{\varepsilon} = k_4\left(D_{gb}/d^2\right)(\sigma/E)^2$ [1]	$k_4 = 1.5 \times 10^3$
Slip Creep (Climb)	$\dot{\varepsilon} = k_5\left(D_L/b^2\right)(\sigma/E)^5$ [2]	$k_5 = 3.7 \times 10^8$
Slip creep (Climb-PLB)	$\dot{\varepsilon} = k_8\{\sinh[\alpha(\sigma/E)]\}^5\left(D_L/b^2\right)(b/d)^p$ [3]	$p = 0.4$, $\alpha = 714$ $k_8 = 1.3 \times 10^{-4}$

$D_L = 1 \times 10^{-4}\exp(-Q_L/RT)$ (m^2/s), with: $Q_L = 135$ (kJ/mol).
$D_{gb} = D_{0,gb}\exp(-Q_{gb}/RT)$ (m^2/s), with: $D_{0,gb} = 5 \times 10^{-12}/2b$ and $Q_{GB} = 92$ (kJ/mol).
$b = 3.21 \times 10^{-10}$ (m), $E = 43{,}000[1-(5 \times 10^{-4}(T - 300))]$ [MPa] Ref. [21].
R is the gas constant, d is the true Grain size, b is Burgers vector, p and α are material parameters, and E is the Young modulus.

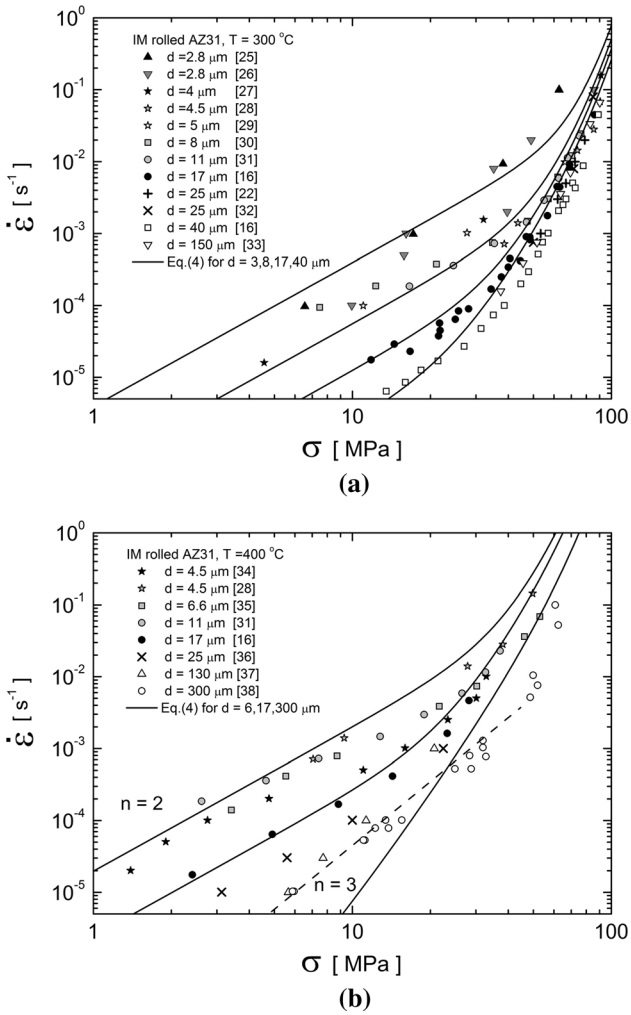

Fig. 7—Strain rate *vs* flow stress data. (*a*) IM-rolled AZ31 at 300 °C. (*b*) IM-rolled AZ31 at 400 °C.

and only initial or final grain sizes are given in most literature studies. The effects of these microstructural variations were highlighted in Figure 1 of Reference 21; for example, experimental results show a variation of k_4 between 2.6×10^2 and 6.5×10^3, with an intermediate value of $k_4 = 1.5 \times 10^3$.

C. *Quantitative Evaluation of the Creep Data for PM and PMCM Materials According to the Graphical Method*

Going back to the analysis of the creep behavior of PM and PMCM materials, in the literature[11–13,15,17,39] when data such as those shown in Figures 6(a) through (c) are analyzed, two assumptions are undertaken. The first is that the creep occurs by GBS, and the second is that the downward curvature of the data is due to the occurrence of a threshold stress, σ_{th}, which may be included in Eq. [1] as follows[39]:

$$\dot{\varepsilon} = k_4 \left(D_{gb}/d^2\right)\left[(\sigma - \sigma_{th})/E\right]^2 \qquad [5]$$

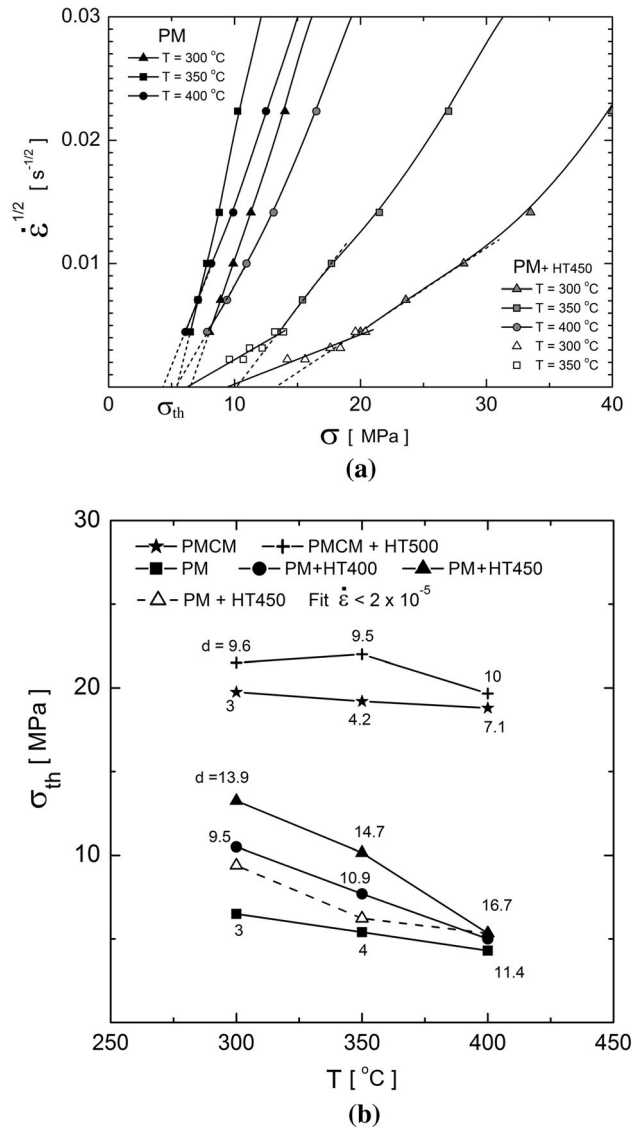

Fig. 8—(*a*) Linear fits performed between 2×10^{-5} and 1×10^{-4} s^{-1} (dashed lines) leading to a set of threshold stresses for PM samples. Measurements made at very low strain rates, in the range 5×10^{-6} s^{-1} up to 2×10^{-5} s^{-1} (open symbols), yield lower values of σ_{th}. (*b*) Threshold stresses obtained by the linear extrapolation are shown as a function of temperature and grain size for PM and PMCM samples.

To obtain the threshold stress, a graphical method derived from Eq. [5] is used in most works. The square root of the strain rate is plotted as a function of the stress, a linear fit is performed, and the threshold stress is obtained by an extrapolation to zero strain rate. Figure 8(a) shows the determination of the threshold stresses by this graphical method for PM samples, and Figure 8(b) shows the threshold stress obtained for PM and PMCM materials.

For each test temperature, the grain size, measured after testing, has been indicated for each point.

The result of applying this data analysis is that the obtained threshold stress is dependent on temperature

and grain size. Moreover, the dependence on these parameters should be different for PM and PMCM samples: The results of Figure 8 would lead to conclude that there is a small dependence on grain size and temperature in PMCM samples, while there is a large grain size and temperature dependence on the threshold stress for the PM material. Furthermore, for the same grain size and temperature, PMCM samples have a threshold stress that is more than double that for PM samples. This could only be accepted as a phenomenological approach since there is no theoretical model that allows rationalization of this dependency.

In addition to the difficulties encountered in interpreting these results, it is possible to make various criticisms of the method of analysis by means of Eq. [5]. First, the procedure of calculating the threshold stress at each temperature by plotting $\dot{\varepsilon}^{1/n}$ *vs* σ is uncertain since many values of n may give the best fit.[40] Second, the method to obtain the threshold stress assumes that the contribution of slip creep can be ruled out. As shown in the previous section, the slip creep equation in Eq. [3] gives a non-negligible contribution in Eq. [4] in the case of medium grain sizes and allows adjustment of the data at high strain rates. This contribution should be taken into account in the study of powder materials, and their effect on the threshold stress should be analyzed.

The third criticism is that the average grain size has been considered sufficient to fully characterize the microstructure of the samples. This may be enough in the case of PMCM samples that are mostly homogeneous, but not in the case of PM samples. The PM material has an inhomogeneous distribution of oxide dispersoids leading to zones of the microstructure with oxides and fine grains and zones free of oxides with larger grains, especially after the annealing thermal treatments. Therefore, the PM material should be properly treated as a composite material, as will be shown in Section IV–F.

D. *Deformation Mechanisms and Threshold Stresses in Cryomilled Samples, PMCM AZ31*

The analysis of PMCM data in terms of the creep equations describing the IM-AZ31 is performed in this section. Figure 9(a) shows the data and the adjusting by Eq. [5] using the parameter $k_4 = 1.5 \times 10^3$ derived from the study of rolled AZ31 (Table II) and the corresponding grain sizes for each sample (Table I; measured in the

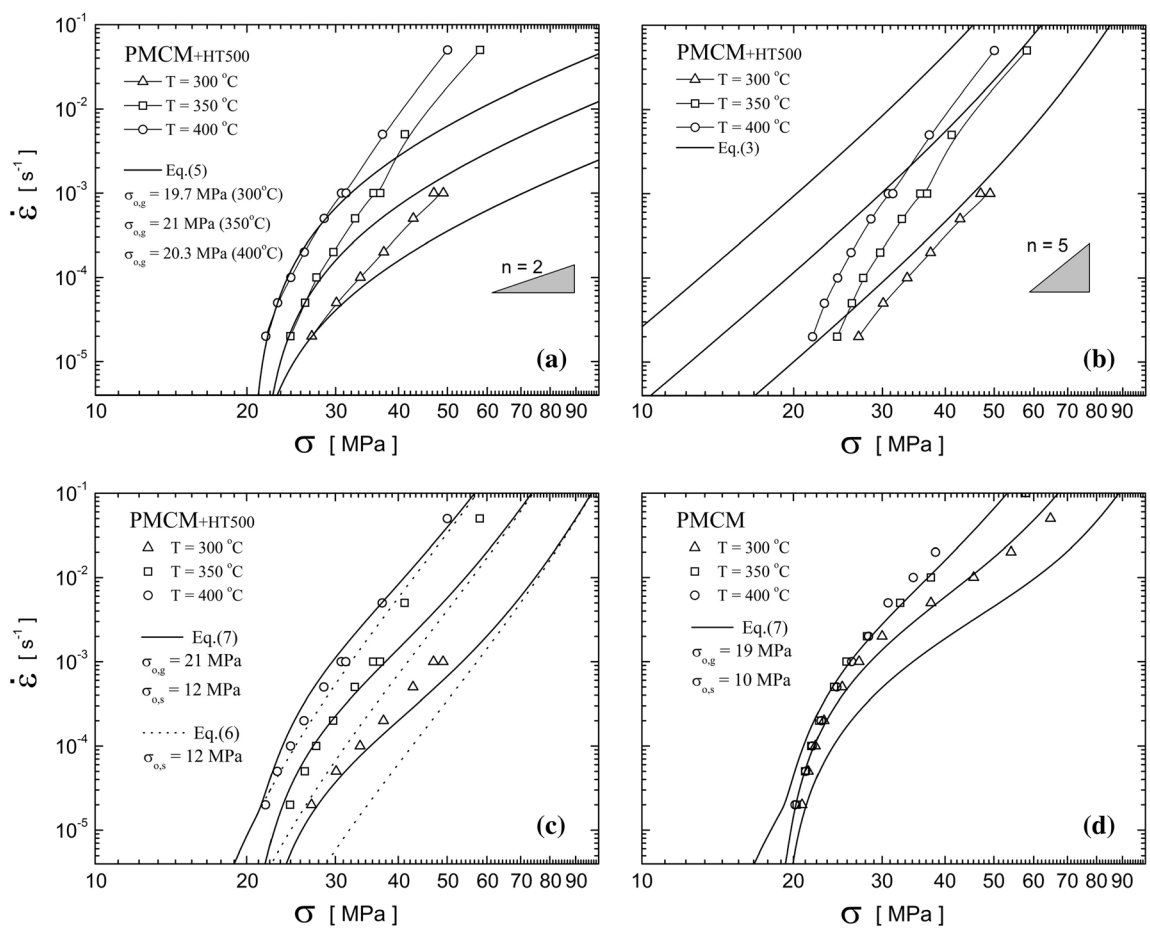

Fig. 9—Strain rate *vs* flow stress data for PMCM AZ31. (*a*) Fitting of Eq. [5] for PMCM + HT500 samples. (*b*) The predicted contribution of the slip creep without threshold stress, Eq. [3]. (*c*) and (*d*) the PMCM data are displayed together with the fit of Eq. [7]; the values of threshold stresses $\sigma_{o,g}$ and $\sigma_{o,s}$ are given.

deformed zone after tensile tests). Data of PMCM material are well adjusted for low strain rates, using σ_{th} = 19.7, 21 and 20.3 MPa for the temperatures 300 °C, 350 °C and 400 °C, respectively. These threshold stresses agree with those of Figure 8(b).

A slip creep contribution will now be taken into account as presented in the IM-AZ31 material, given by Eq. [3], using the corresponding grain sizes for each sample (measured in the deformed zone after tensile tests; Table I) and the parameters of Table II. Figure 9(b) shows the expected contribution of slip creep, according to Eq. [3].

As can be seen, the strain rates due to the slip creep contribution should be much higher than the measured strain rates. That is, if only the GBS is affected by a threshold stress, the dominant deformation mechanism should switch to a slip creep mechanism.

The only reasonable conclusion is that there is a slip creep contribution that is also affected by a threshold stress, named as $\sigma_{o,s}$, in the form:

$$\dot{\varepsilon} = k_8 \left\{ \sinh\left[\alpha\left(\sigma - \sigma_{o,s}\right)/E\right] \right\}^5 \left(D_L/b^2\right) (b/d)^p \quad [6]$$

Therefore, to perform an analysis of the PM AZ31 data, consistent with the results from the conventional rolled AZ31 alloy, *i.e.*, using the same parameters k_4 and k_8, the model should have the following equation:

$$\begin{aligned}\dot{\varepsilon} = {} & k_4 \left(D_{gb}/d^2\right)\left[\left(\sigma - \sigma_{o,g}\right)/E\right]^2 \\ & + k_8 \left\{ \sinh\left[\alpha\left(\sigma - \sigma_{o,s}\right)/E\right] \right\}^5 \left(D_L/b^2\right) (b/d)^p\end{aligned} \quad [7]$$

where two threshold stresses have been differentiated: $\sigma_{o,g}$ for GBS and $\sigma_{o,s}$ for slip creep.

In Figures 9(c) and (d) displays the PMCM data together with the fit of Eq. [7]. The data of PMCM + HT500 were adjusted using $\sigma_{o,g}$ = 21 and $\sigma_{o,s}$ = 12. For PMCM data the model curves were generated with slightly lower values: $\sigma_{o,g}$ = 19 MPa and $\sigma_{o,s}$ = 10 MPa. The fittings of the experimental data were very good. The data for PMCM samples at 300 °C were slightly higher than predicted by the model, probably due to the current grain size during testing, which is slightly lower than that measured after the tests.

Two important observations are derived from this analysis. First, data can be adjusted using the set of constitutive equations for creep in IM-rolled AZ31 with the introduction of two threshold stresses, $\sigma_{o,g} = 20 \pm 1$ MPa and $\sigma_{o,s} = 11 \pm 1$ MPa, for GBS and slip creep respectively. Second, these stresses are independent of grain size and temperature.

The effect of particles on slip creep controlled by the dislocation climb mechanism has been modeled by Arzt *et al.*[19,20] One of their most significant results is the appearance of a threshold stress associated with the attraction between dislocations and particles. The threshold stress, related to detachment of dislocations, is given by:

$$\tau_d = \tau_O \sqrt{1 - k^2} \quad [8]$$

where k is the "relaxation factor" of the dislocation line energy in the particle interface and τ_o is the Orowan by pass stress. As is usually recognized,[41–43] the experimental measurements of the macroscopic detachment stress show that it is a fraction of σ_O, the macroscopic Orowan stress, in the range:

$$\sigma_d = (0.4 \ldots 0.7)\sigma_O \quad [9]$$

This macroscopic detachment stress should correspond to our $\sigma_{o,s}$. Taking into account that the threshold stress for GBS is almost twice the threshold stress for slip, this means that $\sigma_{o,g}$ should be close to the Orowan by pass stress:

$$\sigma_{0,g} \approx 2\sigma_{0,s} \approx \sigma_O \quad [10]$$

It is worth noting that although this model seems to be appropriate to explain the origin of the threshold stresses, its predictions are not always consistent with the experimental data. A quantitative analysis would therefore be pertinent.

E. *Deformation Mechanisms and Threshold Stresses in PM AZ31*

As mentioned in Sections IV–A and IV–C, the as-extruded PM and PMCM samples have the same grain size, and the comparison between both materials in Figure 6(a), gives a clue about the role of oxide dispersoids. From Figure 6(b) indicates that threshold stresses are practically not dependent on grain size since the grain growth produced by the annealing treatment does not affect the threshold stresses mostly in PMCM samples.

However, Figures 6(c) and 8(b) show that the effect of the annealing treatment is strong in the PM material. At first glance, if the experimental results of the PMCM material were not known, it could be concluded that there is a strong grain size and temperature effect on the threshold stress in the PM material. However, it will be shown, that the variation in threshold stress should be attributed to the particularities of the microstructure of the PM AZ31 material instead of a change of the deformation mechanism. The PM material has a heterogeneous distribution of oxide dispersoids leading to zones of the microstructure with oxides and fine grains and zones free of oxides with larger grains. Therefore, the PM material should be properly treated as a composite material.

In the following, the model used in Section D will be modified to deal with this PM material. As shown in Figure 3, the PM AZ31 can be considered as composed of two phases, one containing grains with oxide particles and the other with grains free of oxide particles. These two phases are stretched along the extrusion direction, which is parallel to the tensile axis in the mechanical tests. Therefore, the deformation model for this composite material should consider that each phase deforms at the imposed macroscopic strain rate, *i.e.*, an isostrain condition should be assumed:

$$\dot{\varepsilon} = \dot{\varepsilon}_{ox} = \dot{\varepsilon}_f \quad [11]$$

where $\dot{\varepsilon}_{ox}$ is the strain rate of the phase containing oxide particles and $\dot{\varepsilon}_f$ is the strain rate of the phase free of them. In each phase, the strain rate is a function of the respective stress given by the constitutive equations:

$$\dot{\varepsilon}_{ox} = k_4 \left(D_{gb}/d_{ox}^2\right)\left[\left(\sigma_{ox} - \sigma_{o,g}\right)/E\right]^2 + k_8 \left\{ \sinh\left[\alpha\left(\sigma_{ox} - \sigma_{o,s}\right)\right)/E\right] \right\}^n \left(D_L/b^2\right) \left(b/d_{ox}\right)^p \quad [12]$$

$$\dot{\varepsilon}_f = k_4 \left(D_{gb}/d_f^2\right)\left[\sigma_f/E\right]^2 + k_8 \left\{ \sinh\left[\alpha\,\sigma_f/E\right] \right\}^n \left(D_L/b^2\right) \left(b/d_f\right)^p \quad [13]$$

where two grain sizes are differentiated, d_{ox} and d_f, for the case that each phase has a different grain size. Furthermore, the deformation of the phase free of oxide particles is not affected by a threshold stress, Eq. [13]. The stress supported by these phases contributes to the overall stress σ weighted with their volume fraction[44,45]:

$$\sigma = f_{ox}\,\sigma_{ox} + (1 - f_{ox})\,\sigma_f \quad [14]$$

The procedure to obtain a curve ($\dot{\varepsilon}$, σ) is as follows: for a given input value of $\dot{\varepsilon}$, the stresses σ_{ox} and σ_f are numerically computed for each phase using Eqs. [12] and [13]. The total flow stress σ is next calculated with Eq. [14] using the respective volume fractions. In Figure 10, the stresses σ_{ox}, σ_f and the resulting stress σ calculated with Eqs. [12] through [14] are shown for a set of parameters: T = 350 °C, $d_{ox} = d_f$ = 3 μm, f_{ox} = 0.25, $\sigma_{o,g}$ = 20 MPa and $\sigma_{o,s}$ = 10 MPa.

It is interesting to realize that the threshold stress for creep in the composite material is derived in a straightforward way. As the strain rate decreases, the stress contribution of the soft phase decreases more quickly, and eventually $f_{ox}\sigma_{ox} >> (1 - f_{ox})\sigma_f$. Therefore, the stress of the composite practically reduces to the contribution of the hard phase $\sigma \approx f_{ox}\sigma_{ox}$. As shown in Figure 10, when σ_{ox} tends to the threshold stress $\sigma_{th} = \sigma_{o,g} \approx 20$ MPa, the stress of the composite material tends to be f_{ox}20 MPa. At even lower rates when the curve tends to $\sigma_{th} = \sigma_{o,s} \approx 10$ MPa, the stress of the composite material tends to be approximately f_{ox}10 MPa.

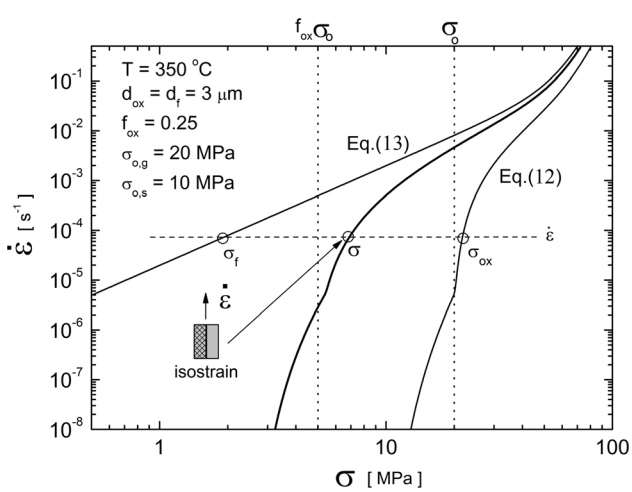

Fig. 10—Example of the calculation method of the strain rate *vs* stress curve from the curves of the material without threshold stress (Eq. [13]) and of the material with threshold stress (Eq. [12]) using an isostrain composite model and the set of parameters: T = 350 °C, $d_{ox} = d_f$ = 3 μm, f_{ox} = 0.25, $\sigma_{o,g}$ = 20 MPa and $\sigma_{o,s}$ = 10 MPa.

The procedure to analyze the experimental data seems complicated, but it benefits from the knowledge of almost all the parameters of the model thanks to the previous study carried out in IM AZ31 and in the PMCM samples:

1. The parameters, k_4 and k_8, and the diffusivities, α and p, will be those previously used.
2. The threshold stresses are derived from the analysis of the PMCM material. It was found that: $\sigma_{o,g}$ = 20 ± 1 MPa and $\sigma_{o,s}$ = 11 ± 1 MPa.
3. Grain sizes, d_{ox} and d_f, for each phase were determined by optical microscopy and are given in Table I. The model was also applied by testing average grain size $d_{ox} = d_f$ = d.
4. The volume fraction f_{ox} can be estimated from microstructural studies. From optical micrographs, the volume fraction of those areas with small grains characteristic of the presence of oxides can be measured. An estimation of about 0.2 is derived. Moreover, from Figure 8(b) the threshold stresses for the PMCM and PM materials were determined to be close to 20 and 5 MPa, respectively. Taking into account that the composite model predicts a threshold stress of $f_{ox}\sigma_{th}$ for the PM material, a volume fraction f_{ox} close to 0.25 is expected, in good agreement with the experimental data.

In Figures 11(a) through (c), the PM material data are displayed together with the fit of the composite model calculated with Eqs. [11] through [14]. The model was calculated using f_{ox} = 0.25, $\sigma_{o,g}$ = 21 MPa and $\sigma_{o,s}$ = 12 MPa. The grain sizes determined for each phase, d_{ox} and d_f, given in Table I and Figure 11, were used in Eqs. [12] and [13]. In Figure 11(d) the mean grain size was used to calculate the model curves instead of differentiating grain sizes for each phase.

The match between the isostrain model and experimental data is very good considering the restrictions of the parameters and use of the same values of threshold stresses for the complete data set. The influence of taking mean grain sizes or differentiated grain sizes for each phase is not critical, although the adjustment seems slightly better with the use of differentiated grain sizes (Figures 11(c) against (d)).

F. *On the Supposed Dependence of the Threshold Stress on Temperature*

A remarkable feature of the model represented by Eq. [7] is that determination of a single threshold stress, made by a method of linear regressions, gives stresses apparently dependent on temperature. In this section, our analysis explains why determinations performed by the method of linear regressions in representations $\dot{\varepsilon}^{1/2}$ *vs*

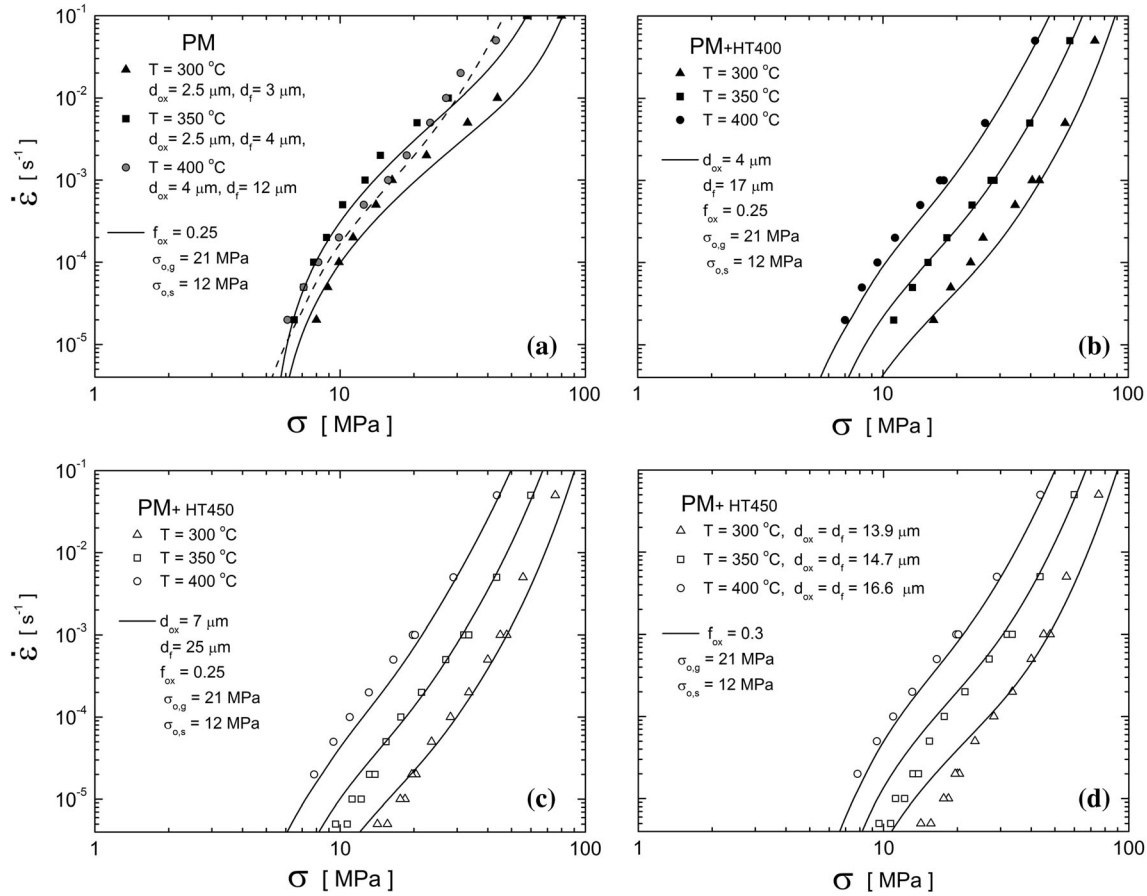

Fig. 11—Strain rate *vs* flow stress data for PM material and the composite model calculated with Eqs. [11] through [14]. (*a*) As extruded material, (*b*) PM + HT400 samples, and (*c*) and (*d*) PM + HT450 samples. The parameters used in the model are given in the graphs. In (d), a mean grain size was used to calculate the model curves instead of different grain sizes for each phase.

σ led to an apparent dependence on the temperature and grain size of the threshold stress.

For this purpose, in Figure 12(a) strain rate *vs* flow stress curves were generated with Eq. [7] for various temperatures. The respective linear fits performed on representations $\dot{\varepsilon}^{1/2}$ *vs* σ are shown in Figure 12(b).

The addition of mechanisms in Eq. [7] causes the curvature of the data at low stresses, Figure 12(b). Since experimental data are not usually measured at sufficiently low stresses to appreciate such curvature, linear extrapolations, as those made in Figures 8(a) and 12(b), result in apparent dependencies of σ_{th} on temperature, shown in the insert of Figure 12(b). Additionally, in the case of PM AZ31, the model given by Eqs. [11] through [14] also leads to threshold stresses dependent on temperature in determinations by the linear regression method. Figure 13(a) shows curves that converges to an unique threshold stress of $f_{ox}\sigma_{o,s} = 2.5$ MPa. Since experimental data are not usually measured at sufficiently low stresses to appreciate such curvature, linear extrapolations, as those made in Figure 8(a), result in an apparent temperature dependence. For the composite material, the temperature and grain size dependence of the apparent threshold stress is larger than in the homogeneous material, as shown in the inserts in Figures 12(b) and 13(b).

In summary, data for the PM AZ31 material can be adjusted using a composite model based on the same constitutive equations for creep found in PMCM AZ31, including the same values of the threshold stresses, $\sigma_{o,g}$ and $\sigma_{o,s}$, and slip creep, respectively, and a realistic set of microstructural parameters. This demonstrates that it is not necessary to invoke a set of threshold stresses that depend on the grain size or the temperature to explain the experimental results in PM materials processed by different routes.

V. CONCLUSIONS

The creep behavior of two powder metallurgical materials, based in the AZ31 magnesium alloy, has been analyzed. The first material, PM AZ31, obtained by extrusion of the alloy powders, presents a heterogeneous distribution of oxide dispersoids in the microstructure. For the second material, PMCM AZ31, the metal powder was previously cryomilled, leading to a homogeneous microstructure. In addition, static annealing treatments give a clue about the role of grain size in both materials. The data presented allowed us to investigate the effect of the main microstructural features, grain size and oxide dispersion on the creep

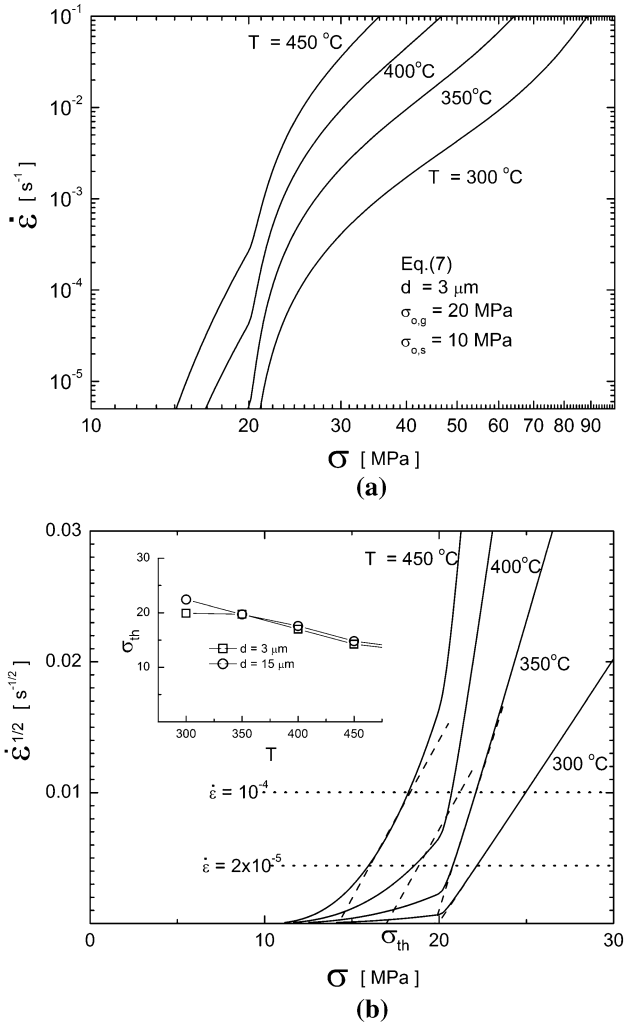

Fig. 12—(*a*) Strain rate *vs* flow stress curves generated with Eq. [7] for various temperatures. (*b*) Representation $\dot{\varepsilon}^{1/2}$ *vs* σ; the linear fits performed between 2×10^{-5} and 1×10^{-4} s^{-1} leads to threshold stresses dependent on temperature.

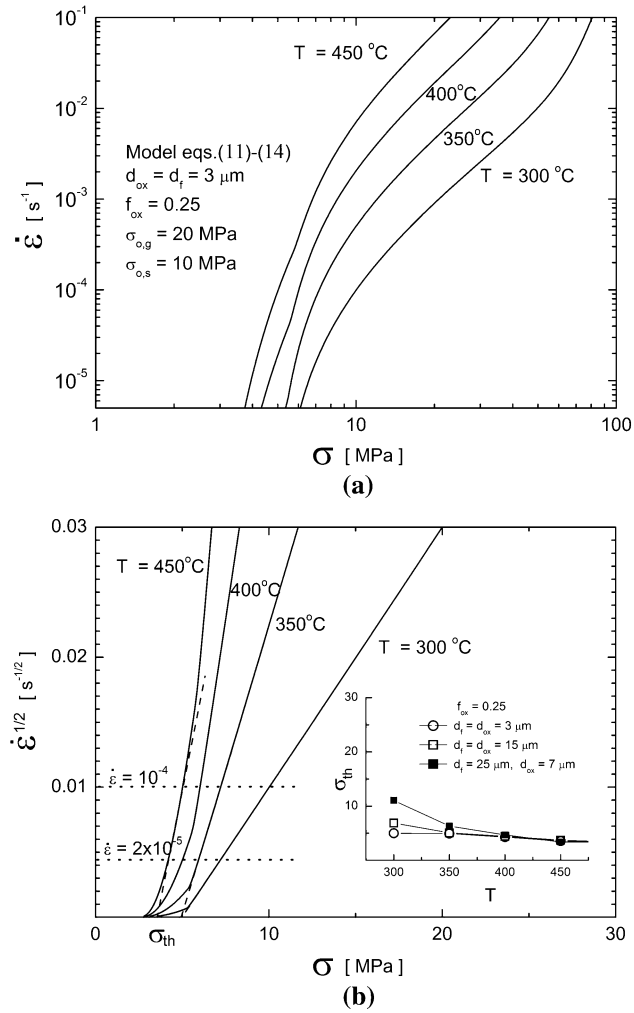

Fig. 13—(*a*) Strain rate *vs* flow stress curves generated with Eqs. [11] through [14] for various temperatures. (*b*) Representation $\dot{\varepsilon}^{1/2}$ *vs* σ; the linear fits performed between 2×10^{-5} and 1×10^{-4} s^{-1} lead to threshold stresses dependent on temperature and grain size.

behavior of powder metallurgy materials. A novel approach avoiding the use of a threshold stress for each temperature and grain size is introduced

First, it is shown that the creep laws of rolled AZ31 were able to describe the results of the PMCM samples by introducing one single constant threshold stress for each of the mechanisms contributing to the deformation rate, GBS and slip creep, namely $\sigma_{o,g} = 20 \pm 1$ MPa and $\sigma_{o,s} = 11 \pm 1$ MPa, respectively. According to the Arzt-Rossler model, the threshold stress for slip creep, $\sigma_{o,s}$, is a fraction of the Orowan stress; therefore, it was concluded that the threshold stress for GBS is close to the Orowan stress.

Regarding the PM AZ31 samples having a heterogeneous microstructure, it was found that the decrease in threshold stresses, compared with PMCM samples, is explained exclusively by the differences in the microstructure homogeneity without the need to invoke a threshold stress depending on grain size or temperature. Creep data can be modeled considering the material as a compound of a soft phase without dispersoids together with a hard phase with dispersoids under an isostrain condition. In this way, data can be adjusted using the same constitutive equations for creep found in PMCM AZ31, with the same constant values of $\sigma_{o,g}$ and $\sigma_{o,s}$. Additionally, our analysis explains why determinations performed by the linear regression method in representations $\dot{\varepsilon}^{1/2}$ *vs* σ lead to an apparent dependence on the temperature and grain size of the threshold stress.

ACKNOWLEDGMENTS

The authors acknowledge the financial support of CICYT, Spain, under Programs MAT2012-38962 and MAT2015-68919 (MINECO/FEDER).

REFERENCES

1. B.L. Mordike and T. Erbert: *Mater. Sci. Eng. A*, 2001, vol. 302, pp. 37–45.
2. I.J. Polmear: *Light Alloys*, 3rd ed., Arnold, London, 1995.
3. *Magnesium and Magnesium Alloys*, M.M. Avedesian, H. Baker, eds., ASM International, 1999.
4. I.A. Anyanwu, S. Kamado, and Y. Kojima: *Mater. Trans.*, 2001, vol. 42, pp. 1206–11.
5. T. Mohri, M. Mabuchi, N. Saito, and M. Nakamura: *Mater. Sci. Eng. A*, 1998, vol. 257, pp. 287–94.
6. K. Yu, W. Li, J. Zhao, Z. Ma, and R. Wang: *Scripta Mater.*, 2003, vol. 48, pp. 1319–23.
7. K. Amiya, T. Ohsuna, and A. Inoue: *Mater. Trans.*, 2003, vol. 44, pp. 2151–56.
8. J. Rao, K. Inoue, and Y. Kawamura: *Adv. Eng. Mater.*, 2005, vol. 7, pp. 507–12.
9. M. Yamasaki, T. Anan, S. Yoshimoto, and Y. Kawamura: *Scripta Mater.*, 2005, vol. 53, pp. 799–803.
10. Q. Li, Q. Wang, H. Zhou, X. Zeng, Y. Zhang, and W. Ding: *Mater. Lett.*, 2005, vol. 59, pp. 2549–54.
11. H. Watanabe, T. Mukai, M. Mabuchi, and K. Higashi: *Acta Mater.*, 2001, vol. 49, pp. 2027–37.
12. H. Watanabe, T. Mukai, K. Ishikawa, T. Mohri, M. Mabuchi, and K. Higashi: *Mater. Trans.*, 2001, vol. 42, pp. 157–62.
13. H. Watanabe, T. Mukai, K. Ishikawa, M. Mabuchi, and K. Higashi: *Mater. Sci. Eng. A*, 2001, vol. 307, pp. 119–28.
14. T.G. Nieh, A.J. Schwartz, and J. Wadsworth: *Mater. Sci. Eng. A*, 1996, vol. 208, pp. 30–36.
15. M. Mabuchi and K. Higashi: *Philos. Mag. A*, 1996, vol. 74, pp. 887–905.
16. J.A. del Valle, M.T. Pérez-Prado, and O.A. Ruano: *Metall. Mater. Trans. A*, 2005, vol. 36A, pp. 1427–38.
17. H. Watanabe, T. Mukai, and K. Higashi: *Metall. Mater Trans. A*, 2008, vol. 39A, pp. 2351–62.
18. A. Ball and M.M. Hutchison: *Met. Sci. J.*, 1969, vol. 3, pp. 1–7.
19. E. Arzt and D.S. Wilkinson: *Acta Metall.*, 1986, vol. 34, pp. 1893–96.
20. E. Arzt and J. Rösler: *Acta Metall.*, 1988, vol. 36, pp. 1053–60.
21. S. Spigarelli, O.A. Ruano, M. El Mehtedi, and J.A. del Valle: *Mater. Sci. Eng. A*, 2013, vol. 570, pp. 135–48.
22. J.A. del Valle and O.A. Ruano: *Mater. Sci. Eng. A*, 2008, vol. 487, pp. 473–80.
23. J.A. del Valle and O.A. Ruano: *Acta Mater.*, 2007, vol. 55, pp. 455–66.
24. J.A. del Valle, F. Peñalba, and O.A. Ruano: *Mater. Sci. Eng. A*, 2007, vol. 467, pp. 165–71.
25. Q.F. Wang, X.P. Xiao, J. Hu, W.W. Xu, X.Q. Zhao, and S.J. Zhao: in *Proc. Sino-Swedish Structural Materials Symposium*, 2007, pp. 167–72.
26. H.K. Lin and J.C. Huang: *Mater. Trans.*, 2002, vol. 43, pp. 2424–32.
27. M. Mabuchi, Y. Chino, and H. Iwasaki: *Mater. Trans.*, 2003, vol. 44, pp. 490–95.
28. D.L. Yin, K.F. Zhang, G.F. Wang, and W.B. Han: *Mater. Lett.*, 2005, vol. 59, pp. 1714–18.
29. H. Watanabe, T. Mukai, K. Ishikawa, Y. Okanda, M. Kohzu, and K. Higashi: *J. Jpn. Inst. Light Met.*, 1999, vol. 49, pp. 401–04.
30. H. Somekawa, H. Watanabe, T. Mukai, and K. Higashi: *Scripta Mater.*, 2003, vol. 48, pp. 1249–54.
31. H. Somekawa, H. Watanabe, and K. Higashi: *Mater. Trans.*, 2003, vol. 44, pp. 496–503.
32. H. Takuda, T. Morishita, T. Kinoshita, and N. Shirakawa: *J. Mater. Process. Technnol.*, 2005, vols. 164–165, pp. 1258–62.
33. W.J. Kim, S.W. Chung, C.S. Chung, and D. Kum: *Acta Mater.*, 2001, vol. 49, pp. 3337–45.
34. F.K. Abu-Farha and M.K. Khraisheh: *Adv. Eng. Mater.*, 2007, vol. 9, pp. 777–83.
35. W.J. Kim, J.D. Park, and U.S. Yoon: *J. Alloys Compd.*, 2008, vol. 464, pp. 197–204.
36. M. Liu, G. Yuan, Q. Wang, Y. Wei, W. Ding, and Y. Zhu: *Mater. Trans.*, 2002, vol. 43, pp. 1–4.
37. H. Watanabe, H. Tsutsui, T. Mukai, M. Kohzu, S. Tanabe, and K. Higashi: *Int. J. Plast*, 2001, vol. 17, pp. 387–97.
38. X. Wu and Y. Liu: *Scripta Mater.*, 2002, vol. 46, pp. 269–74.
39. N. Dua, A.F. Bower, P.E. Krajewski, and E.M. Taleff: *Mater Sci. Eng. A*, 2008, vol. 494, pp. 86–91.
40. A. Yawny and G. Eggeler: *Mater. Sci. Eng. A*, 2004, vols. 387–389, pp. 905–09.
41. L.M. Brown and R.K. Ham: in *Strengthening Methods in Crystals*, A. Kelly, R. B. Nicholson, eds., Elsevier, Amsterdam, 1971.
42. R.S.W. Shewfelt and L.M. Brown: *Philos. Mag.*, 1977, vol. 35, pp. 945–62.
43. J. Rösler and E. Arzt: *Acta Metall.*, 1988, vol. 36, pp. 1043–51.
44. A.K. Ghosh and R. Raj: *Acta Metall.*, 1981, vol. 29, pp. 607–16.
45. J.A. del Valle and O.A. Ruano: *Mater. Lett.*, 2008, vol. 62, pp. 3391–94.

Publisher's Note Springer Nature remains neutral with regard to jurisdictional claims in published maps and institutional affiliations.